JOURNAL OF Applied Polymer SCIENCE

Poly(*p*-phenylene sulfide) Nanofibers Prepared by CO_2 Laser Supersonic Drawing

Hiroyuki Koyama, Yuta Watanabe, Akihiro Suzuki
Interdisciplinary Graduate of School of Medicine and Engineering, University of Yamanashi, Takeda-4, Kofu 400-8511, Japan
Correspondence to: H. Koyama (E-mail: koyama@nissan-arc.co.jp)

ABSTRACT: Poly(*p*-phenylene sulfide) (PPS) nanofibers are prepared by irradiating a PPS fiber with a carbon dioxide (CO_2) laser while drawing it at supersonic speeds. A supersonic jet is generated by blowing air into a vacuum chamber through the fiber injection orifice. Nanofibers obtained at a laser power of 30 W and chamber pressure of 10 kPa exhibit an average diameter of 600 nm and a draw ratio of 110,000. Scanning electron microscopy, differential scanning calorimetry, and wide-angle X-ray diffraction analyses are employed to investigate the relationships among the chamber pressure, fiber morphology, and crystallization behavior. The nanofibers exhibit two melting temperatures (T_m): approximately 280°C and 320°C. The endothermic peak at $T_m = 280$°C is ascribable to lamellar crystals and that at $T_m = 320$°C to the highly complete crystals, since the polymer molecular chain is highly oriented. © 2014 Wiley Periodicals, Inc. J. Appl. Polym. Sci. **2014**, *131*, 40922.

KEYWORDS: morphology; nanoparticles; nanostructured polymers; nanowires and nanocrystals

Received 16 December 2013; accepted 26 April 2014
DOI: 10.1002/app.40922

INTRODUCTION

Poly(*p*-phenylene sulfide) (PPS) is being used widely in the electrical, automotive, medical, and chemical industries because of its excellent thermal stability and high chemical resistance.[1,2] Similarly, nanofibers also find wide application in a number of areas, including in the manufacture of membranes, biomedical devices, and tissue engineering scaffolding.[3–5] It is thus logical that nanofibers of PPS would be useful in a wide variety of fields as highly functional components. Nanofibers can be produced by a number of techniques, such as electrospinning,[6–13] melt electrospinning,[14–16] sea-island-type conjugate melt spinning, melt blowing,[17,18] spunbonding,[19] and jet blowing.[20] In the area of super engineering plastics, polyethylene terephthalate (PET) and Nylon 6 nanofibers are usually prepared by electrospinning and sea-island-type conjugate melt spinning.[21,22] However, these techniques are not very environmentally friendly, as they require the use of solutions that are not biodegradable, and involve multiple processing steps.

In this study, we investigated a new approach for preparing PPS nanofibers through carbon dioxide (CO_2) laser-based supersonic drawing (CLSD). There have been a few previous reports on the fabrication of continuous PPS nanofibers. When using CLSD to fabricate continuous nanofibers, one does not require additional solutions or processes. The underlying mechanism involves the irradiation of a PPS fiber with a CO_2 laser while it is being drawn from a supersonic jet. CLSD has already been used to fabricate nanofibers of poly(L-lactic acid) (PLLA)[23] and polyethylene-2,6-naphthalate.[24] However, the challenge in using the CLSD technique to fabricate PPS nanofibers is that the chemical and heat resistances of PPS are higher than those of the materials that have been previously drawn using the technique. For example, PPS does not dissolve readily in any solvent at room temperature, and, owing to its high melting point (280°C) requires a large amount of heat to melt. In addition, in its molten form, the polymer exhibits high flow behavior and low viscosity. Therefore, the fabrication of continuous nanofibers of PPS using conventional methods requires that the molten polymer undergo solidification instantly, that is, as soon as it is drawn. As a result, it is difficult to produce continuous nanofibers of PPS using conventional methods. With CLSD, one can overcome these issues, because PPS is melted by laser irradiation while being drawn by air jets at supersonic speeds, and then quenched at a lower temperature. Thus, CLSD is a new route for fabricating nanofibers of various materials. Even though nanofibers of various materials can be produced by other techniques as well, CLSD is particularly suited for fabricating PPS nanofibers.

We determined the velocity and temperature distributions of the air jet emanating from the orifice using fluid mechanics analyses based on the three-dimensional finite element method (3D FEM). These simulations have been described in a previous article.[25] Table I shows the flow velocities of the air jet,

Table I. Maximum Flow Velocity in the Supersonic Jet at Three Different Chamber Pressures (p_{ch}), as Estimated by 3D FEM-Based Analyses

p_{ch} (kPa)	Maximum flow velocity (m s^{-1})
10	619
30	446
50	324

determined from the simulations; the simulations were performed for chamber pressures of 10, 30, and 50 kPa, while assuming that the diameter of the orifice was 0.5 mm. The flow velocities corresponding to 10 and 30 kPa were in the supersonic range.

The position of the irradiating laser beam, the rate of supply of the molten polymer, the chamber pressure (p_{ch}), and the laser power determine the diameter of the synthesized nanofibers. In particular, the diameter depends strongly on the chamber pressure. Therefore, the relationship between the chamber pressure and the characteristics of the synthesized nanofibers was investigated in depth. In addition, the morphology, thermal behavior, crystallinity, and the molecular chain orientation of the obtained nanofibers were also investigated.

The morphology of the obtained fibers was characterized using scanning electron microscopy (SEM) and an image analyzer; the draw ratio of the fibers was determined from the SEM images. The crystallinity of the fibers was measured using differential scanning calorimetry (DSC), and their molecular chain orientation was determined using wide-angle X-ray diffraction (WAXD) analysis.

Furthermore, the nanofibers were annealed to control the crystal growth and orientation. These characteristics were also investigated, given the effect the post-annealing crystal morphology and orientation of the polymer have on its mechanical properties and dimensional stability.

EXPERIMENTAL

Preparing PPS Fiber for Drawing

The fiber used as the starting material was an as-spun PPS fiber prepared at 300°C using a capillary rheometer (Capilograph ID, Toyo Seiki Seisaku-sho, Ltd., Japan). The PPS used was a linear-type one (FORTRON, Polyplastics Co., Ltd., Japan). The as-spun fiber had a diameter of 201 μm and crystallinity of 17%. The number-average molecular weight (M_n) and weight-average molecular weight (M_w) of the fiber were 11,400 and 63,900, respectively. The molecular weight distribution of the fiber was measured by gel permeation chromatography (GPC) (SSC7100, Senshu Scientific Co., Ltd., Japan) using a solution of 1-chrolonaphthol (1-CN) at 250°C. The GPC-based measurement was performed using a 50 cm gel column and a differential refractive index detector (RID).

CO_2 Laser Supersonic Drawing System

Figure 1 shows the apparatus used for the CLSD process. The apparatus consisted of a spool that supplied the fiber; a continuous-wave CO_2 laser with an output wavelength of 10.6 μm and maximum power of 30 W; an acrylic chamber with Zn-Se windows through which the laser beam was transmitted into the chamber; an orifice, measuring 0.5 mm in diameter, for fiber injection; a power meter; a movable plate that could be moved parallel to the *Y* and *Z* axes; and a vacuum pump. The movable plate could be rotated about the irradiation point on the fiber. The vacuum chamber was placed on the movable plate, and the starting fiber was laser irradiated at a point approximately 3 mm away from the orifice. A supersonic jet was generated by blowing a stream of air into the vacuum

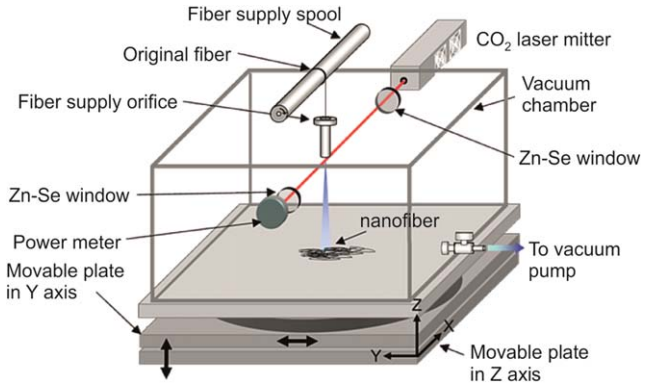

Figure 1. Schematic diagram of the apparatus used for CO_2 laser-based supersonic drawing. [Color figure can be viewed in the online issue, which is available at wileyonlinelibrary.com.]

Figure 2. Photograph of the collected drawn fibers.

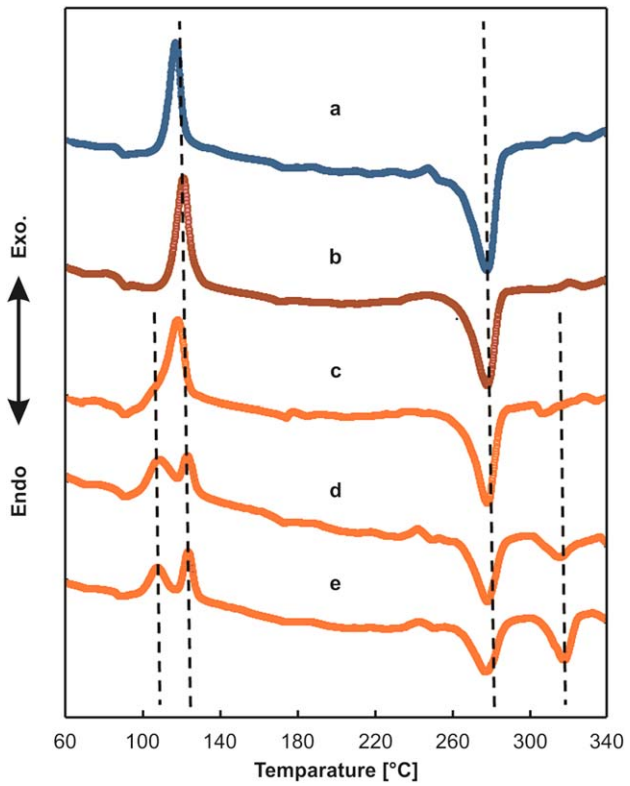

Figure 3. DSC curves for (a) the original fiber and the drawn fibers obtained at chamber pressures (p_{ch}) of (b) 50 kPa, (c) 30 kPa, (d) 20 kPa, and (e) 10 kPa. [Color figure can be viewed in the online issue, which is available at wileyonlinelibrary.com.]

chamber through the orifice used to inject the fiber. The adiabatic expansion of air across the orifice resulted in a drop in temperature of the jet of air, while the fiber was instantly melted by the high-power laser irradiating the cooled supersonic air jet. The supersonic flow generated significantly large shear and compressive forces as well as marked deformation, resulting in draw ratios on the order of 10^5.

The drawn fibers drooped with respect to the draw axis when expelled from the orifice by the supersonic jet. It was easy for us to collect the fibers in a bundle and align them, as shown in Figure 2. We obtained a fabric piece ~2 cm in width and 15 cm in length after drawing for 10 min.

As mentioned previously, annealing was performed to ascertain the crystallization behavior of the synthesized nanofibers. The fibers were placed between two aluminum plates, which held the fabric piece in a fixed position. The fibers were heated to and kept at 250°C for 15 min; the temperature was chosen because it is close to melting point but above the glass transition temperature of PPS. The annealing time was kept at 15 min, as there was no change in the properties for longer periods.

Nanofiber Characterization

The morphology of the synthesized fibers was ascertained using SEM (JSM 6060LV, JEOL Ltd., Japan), performed at an accelerating voltage of 10 kV. An image analyzer was used to determine the average diameter and diameter distribution of the fibers. The average fiber diameter was determined from measurements made at 100 different locations on a webbed fiber. The crystallinity of the nanofibers was determined using DSC (Thermo Plus 2 8230C, Rigaku Co., Japan). The DSC scans were performed within the temperature range of 25–350°C at a heating rate of 10°C min^{-1} in an atmosphere of nitrogen.

Table II. Cold Crystallization Temperatures (T_{cc}), Melting Temperatures (T_m), and Degrees of Crystallinity (χ_c) of the Original Fiber and the Drawn Fibers Obtained at Four Different Chamber Pressures (p_{ch})

Sample	T_{cc} (°C)	T_m (°C)	χ_c (%)
Original	118	278	17.0
p_{ch} = 10 kPa	108/124	278/318	8.0
p_{ch} = 20 kPa	109/123	278/315	5.2
p_{ch} = 30 kPa	118	278	4.2
p_{ch} = 50 kPa	121	278	3.8

Nanofiber Crystallinity

The degree of crystallinity (χ_c) of the nanofibers was determined on the basis of their heat of fusion (ΔH_m) and enthalpy of cold crystallinity (ΔH_{cc}) using the following equation:

$$\chi_c = \frac{(\Delta H_m + \Delta H_{cc})}{-146.2} \times 100 \quad (1)$$

where $\Delta H_m = -146.2$ J g^{-1} for the crystalline phase of PPS.[26]

Characterization of Annealed Fibers

The orientation of the drawn nanofibers was investigated using WAXD analysis. The WAXD patterns of the nanofibers were obtained using an imaging plate (IP) film and an IP detector (R-AXIS DS3C, Rigaku Co., Japan). The IP film was attached to an X-ray generator (Rigaku Co. Japan) operated at 40 kV and 200 mA. The measurements were performed on aligned fiber bundles, which were assumed to be parallel to the draw axis. The annealed fibers were also characterized using SEM. The texture of the annealed nanofibers was determined by etching the fibers in the amorphous phase selectively.[27] The etching was performed using a mixture of anhydrous aluminum chloride in a concentration of 0.8% by weight in toluene. The fibers were etched at 35°C for 16 min in a nitrogen atmosphere. After being etched, the fibers were immersed in methanol for 30 s and rinsed in acetone for 1 min. The etched fibers were then dried at room temperature for 24 h and observed using SEM.

RESULTS AND DISCUSSION

Drawing Conditions

The relationship between the chamber pressure and the characteristics of the drawn fibers was investigated in detail, as the diameter of the fibers depends strongly on the pressure. During this series of experiments, the irradiating laser was held at a constant distance (3 mm) from the fiber-supply orifice, and the fiber was supplied at a steady speed of 0.1 m min^{-1}. It was found in a previous study that, when the shear and compressive forces are at their maximum and a drag force acts on the fiber in the supersonic jet, parallel and perpendicular forces (shear

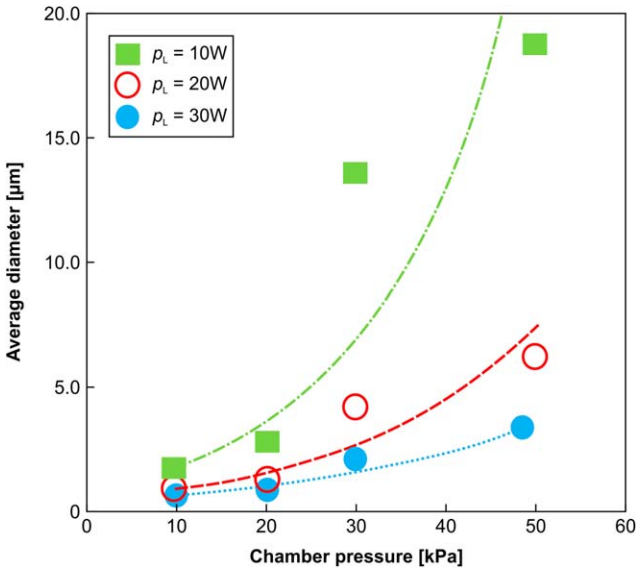

Figure 4. Chamber-pressure dependence of the average diameter of the fibers obtained at three different laser powers. [Color figure can be viewed in the online issue, which is available at wileyonlinelibrary.com.]

and compressive forces, respectively) act on the surface of the fiber.[28] The fiber supply speed of 0.1 m min^{-1} was high enough to deform the molten polymer without resulting in the formation of droplets.

Chamber-Pressure Dependence of Fiber Properties

Figure 3 shows the DSC curves for the fibers obtained at various chamber pressures. In this series of experiment, the laser power used was the maximum possible (30 W). All the fibers exhibited exothermic peaks at approximately 120°C, owing to cold crystallization, and broad endothermic peaks at 278°C, owing to the melting of the crystals. Table II shows the cold crystallization temperatures (T_{cc}), melting temperatures (T_m), and degrees of crystallinity (χ_c) of the fibers synthesized at different chamber pressures. The χ_c values of all the fibers were less than 10% and well below that of the starting material. It is likely that this is because the molten polymer was cooled rapidly and quenched. The fibers produced at $p_{ch} = 30$ kPa exhibited broad exothermic peaks at 118°C. Further, two peaks were observed, at 109°C and 123°C, respectively, in the case of the fibers synthesized at $p_{ch} = 20$ kPa; similarly, two peaks, at 108°C and 124°C, respectively, were observed for those fabricated at $p_{ch} = 10$ kPa.

The shift in T_{cc} to a lower value is attributable to the presence of crystal seeds formed by CLSD.[29] In the case of PET fibers prepared by CLSD, the cold crystallization temperature was also found to shift to a lower value with a decrease in the peak areas.[27] However, the crystallization of the PPS fibers was less extensive than that of the PET ones; the crystallization of PPS also requires more time. The characteristics of PPS differ from those of certain other polymers with benzene rings, such as PET. Even though PPS also has benzene rings in its molecular backbone, the phenylene groups restrict the free rotation of the C—S bond. In addition, higher melting peaks were confirmed at 318 and 315°C in the cases of the nanofibers produced at $p_{ch} = 10$ and 20 kPa, respectively. These higher melting temperatures were close to the equilibrium melting point of PPS ($T_m^0 = 320$°C) as reported by Cheng et al.[30]

During the CLSD process, the molten polymer is pulled along the draw axis, resulting in high deformation, and then quenched. We checked for the existence of crystal seeds and whether the molecular chain was oriented toward the draw axis after being fastened by the seeds. It is possible that the heating involved during the DSC measurements promotes the growth of the crystal seeds along the draw axis. Annealing was performed on the drawn fibers to confirm whether this was the case.

Lu et al. have reported that the higher melting point of PPS is that of crystallized PPS under high pressure.[31] It is likely that the melting point of PPS is higher in this case because of the extended molecular chain of the polymer and the orientation of this chain. The diameters and morphologies of the PPS nanofibers obtained using different chamber pressures were also determined. Figure 4 shows the chamber-pressure dependence of the average fiber diameter.

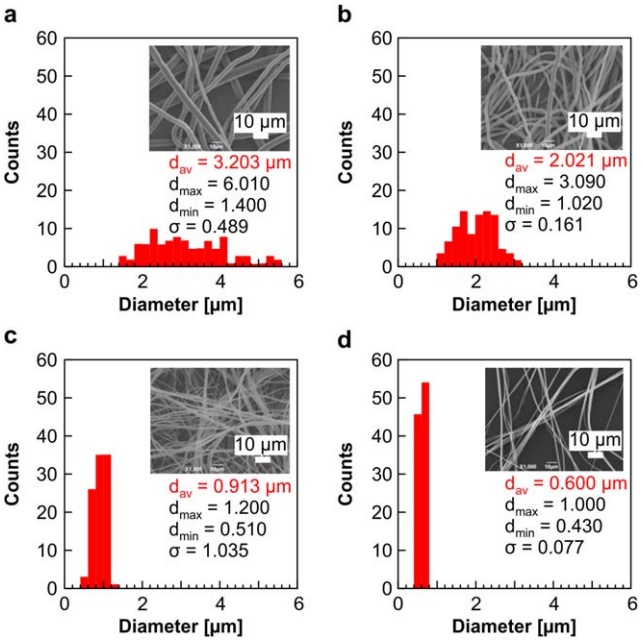

Figure 5. SEM micrographs (magnification: 1000×) and diameter distributions for the fibers obtained at chamber pressures (p_{ch}) of (a) 50 kPa, (b) 30 kPa, (c) 20 kPa, and (d) 10 kPa. [Color figure can be viewed in the online issue, which is available at wileyonlinelibrary.com.]

Table III. Average Diameters (d_{av}) of the Drawn Fibers Obtained at Four Different Chamber Pressures (p_{ch})

Sample	d_{av} (μm)
p_{ch} = 10 kPa	0.600
p_{ch} = 20 kPa	0.913
p_{ch} = 30 kPa	2.021
p_{ch} = 50 kPa	3.203

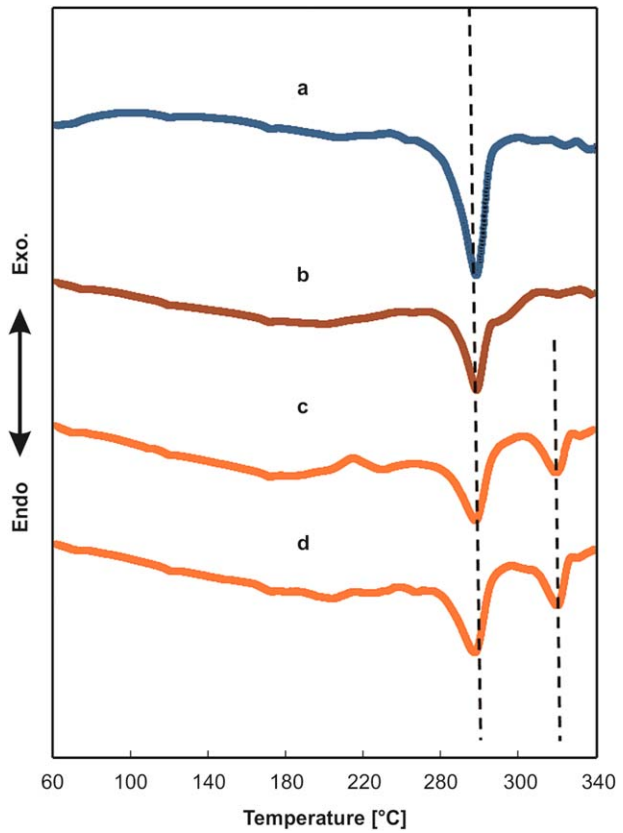

Figure 6. Post-annealing DSC curves for the fibers obtained at chamber pressures (p_{ch}) of (a) 50 kPa, (b) 30 kPa, (c) 20 kPa, and (d) 10 kPa. The DSC scans were performed within the temperature range of 25–350°C at a heating rate of 10 °C min^{-1} in an atmosphere of nitrogen. [Color figure can be viewed in the online issue, which is available at wileyonlinelibrary.com.]

The average diameter decreased significantly as the chamber pressure was decreased and the laser power was increased. It was less than 1 μm at $p_{ch} = 20$ kPa for a laser power of 30 W. Decreasing the chamber pressure would increase the flow velocity of the jet, as well as the drag force in it. This would result in higher plastic deformation of the polymer, producing thinner fibers. Laser powers of 10 W and 20 W were also tried, but it was found that maximum laser power (30 W) was more suitable for obtaining thinner fibers. Figure 5 shows SEM micrographs (magnification: ×1000) and the diameter distribution of the fibers obtained at four different chamber pressures; the laser power was 30 W. The SEM micrographs show that thinner fibers were produced at lower chamber pressures. The fibers exhibited smooth surfaces that were free of droplets. Further, the diameter distribution was more uniform in the case of the thinner fibers.

Table IIIshows average diameters of the drawn fibers obtained at four different chamber pressures.

The thinnest nanofibers obtained at $p_{ch} = 10$ kPa exhibited an average diameter of 600 nm; the standard deviation was 0.077.

Higher flow rates and drag forces resulted in thinner and more uniform nanofibers. The draw ratio (λ) of a drawn fiber can be calculated using the following equation:

Table IV. Degrees of Crystallinity (X_c) of the Drawn and Annealed Fibers Obtained at Four Different Chamber Pressures (p_{ch})

Sample	Drawn fibers (%)	Annealed fibers (%)
p_{ch} = 10 kPa	8.0	26.3
p_{ch} = 20 kPa	5.2	24.1
p_{ch} = 30 kPa	4.2	21.5
p_{ch} = 50 kPa	3.8	20.3

$$\lambda = \left(\frac{d_0}{d}\right)^2 \quad (2)$$

where d_0 is the diameter of the original fiber and d is that of the drawn fiber. The volumes before and after drawing are assumed to be equal. Equation (2) gives a draw ratio of 110,000 at $p_{ch} = 10$ kPa. A very large plastic deformation occurs temporarily during CLSD.

Morphology and Characteristics of Annealed Nanofibers

Figure 6 shows the post-annealing DSC curves for the fibers obtained at the four different chamber pressures. The fibers were heated to and held at 220°C for 15 min. The drawn fibers had exhibited exothermic peaks in the region extending from 100°C to 120°C; however, these peaks were not visible in the case of the annealed fibers. The degree of crystallinity of the annealed fibers was also higher (see Table IV). The annealed fibers had an χ_c value of approximately 25%, which was 10% higher than that of the drawn fibers. It was also higher than that of the starting fiber. In a previous study,[29] PPS microfibers obtained by zone drawing had exhibited an χ_c value of 16%; in addition, these fibers when annealed at 220°C using a zone heater had subsequently exhibited an χ_c value of 38%.

The increase in the χ_c value was owing to crystal seeding and the resulting molecular orientation of the polymer chain, as it was accompanied by a shift in T_{cc} to a lower value. Thus, it can be surmised that flow-induced orientation alignment and crystal seeding occurred during the CLSD process.

Figures 7 and 8 show SEM micrographs and WAXD patterns of the etched nanofibers. The WAXD patterns of the etched fibers exhibited an arc-like reflection, owing to the well-defined orientation of the crystallites; this was true for the fibers obtained at $p_{ch} = 10$, 20, and 30 kPa. These reflections are attributable to the (111/200) plane and correspond to the diffraction peak at $2\theta = 20.5°$, which can be ascribed to the orthorhombic unit cell of crystallized PPS.[32]

The degrees of crystal orientation (π) were estimated from the half widths (H) of the meridian reflection peaks. The π values

Table V. Degrees of Crystal Orientation (π) for the Fibers Drawn at Four Different Chamber Pressures (p_{ch})

Sample	π (%)
p_{ch} = 0 kPa	72
p_{ch} = 20 kPa	88
p_{ch} = 30 kPa	89
p_{ch} = 50 kPa	92

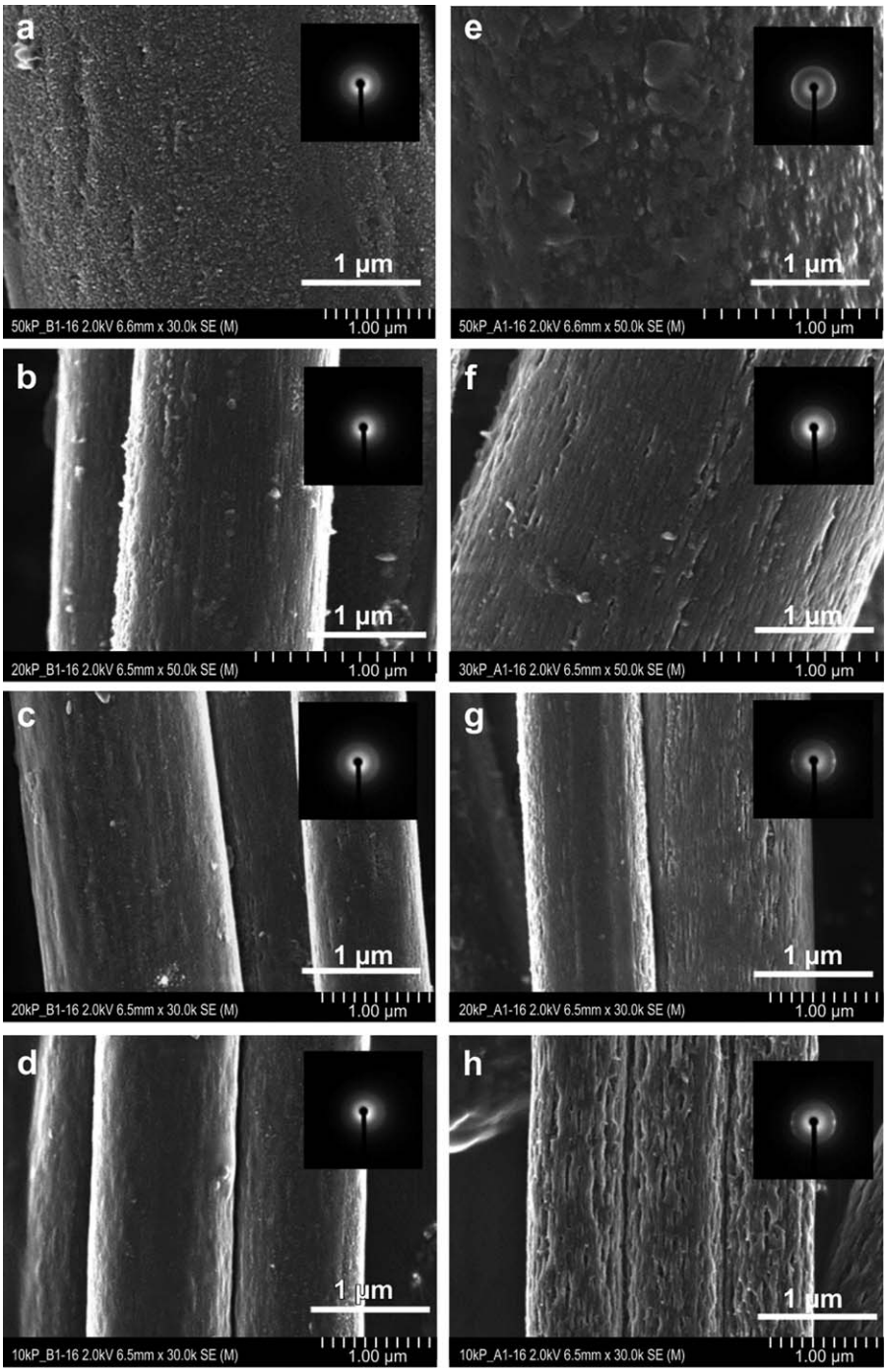

Figure 7. SEM micrographs and WAXD patterns for the etched fibers before and after they were annealed. The images shown correspond to fibers obtained at chamber pressures (p_{ch}) of (a, e) 50 kPa, (b, f) 30 kPa, (c, g) 20 kPa, and (d, h) 10 kPa (Magnification: 30,000×).

were estimated from the WAXD patterns obtained from the imaging plate using data analysis software. The following equation was used to calculate the π values, which are shown in Table V:

$$\pi = \left(\frac{180 - H}{180}\right) \times 100 \quad (3)$$

The results of the WAXD analyses indicated that the obtained fibers were highly oriented along the long axis. Furthermore, the relationship between the WAXD patterns and the morphologies of the etched fibers was also determined.

The surfaces of the etched fibers before they were annealed were smooth, and streaks attributable to the growth of the crystallites were not observed. In addition, the fibers were brittle [see Figure 7(a–d)]. This was because the control fibers consisted almost entirely of the amorphous phase; the acid attacks this phase selectively. However, the surfaces of the etched fibers after

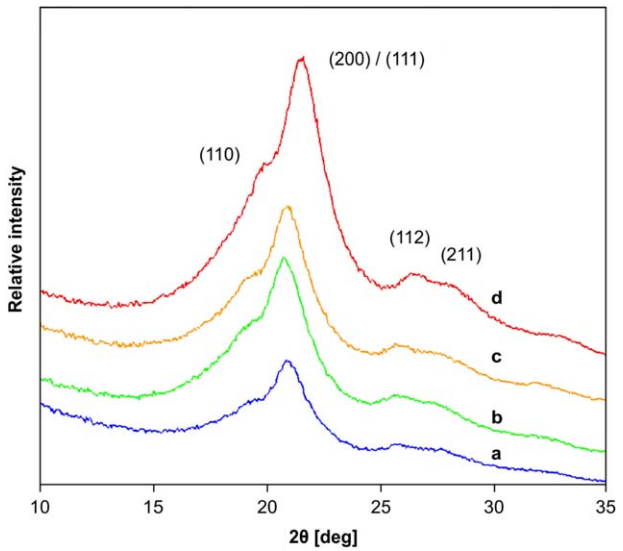

Figure 8. Post-annealing WAXD patterns of the etched fibers obtained at chamber pressures (p_{ch}) of (a) 50 kPa, (b) 30 kPa, (c) 20 kPa, and (d) 10 kPa. [Color figure can be viewed in the online issue, which is available at wileyonlinelibrary.com.]

they had been annealed exhibited signs that proved significant crystallite growth had occurred.

We found that, in the case of the fiber obtained at $p_{ch} = 50$ kPa, the crystallites were randomly oriented, resulting in the nanofiber having a lump-like morphology. The morphologies of the fibers obtained at $p_{ch} = 20$ and 30 kPa were more oriented and band like. In the case of the fiber obtained at $p_{ch} = 10$ kPa, the band-shaped crystallites were significantly oriented along the draw axis. This was further evidence of the growth of oriented crystallites along the draw axis. These results prove that the nanofibers drawn by CLSD exhibited a highly oriented amorphous phase as well as crystal seeds, and that the annealing process resulted in the growth of the crystal seeds along the long axis of the fibers. This phenomenon became more pronounced with a decrease in the chamber pressure. The strong drag forces extend and orient the drawn fibers along the long axis, and annealing promotes the crystallization of the oriented amorphous chains. The high melting points ($T_m = 318$ and 315°C), as determined from the DSC curves, indicated the existence of highly complete crystals.

These results were also suggestive of the possibility of changing the crystal structure of the fibers to one that causes the appearance of another crystal phase or results in thinner, lamellar crystals at high drawing ratios. Therefore, we intend to characterize the nature of crystal packing in the fibers as well as the conformation of the crystals using nuclear magnetic resonance (NMR) and small-angle X-ray scattering (SAXS).

CONCLUSIONS

PPS nanofibers with a uniform diameter were produced using the CLSD technique. The thinnest of the obtained nanofibers had an average diameter of 600 nm (standard deviation of 0.077) when CLSD was performed at a laser power of 30 W, chamber pressure of 10 kPa, fiber supply speed of 0.1 m min^{-1}, and laser-to-fiber distance of 3 mm. The drag forces that are generated in the supersonic jet act on the partially molten polymer. Lower chamber pressures result in stronger drag forces and greater fiber deformation, ultimately resulting in thinner fibers that are oriented along the draw axis. The quenched fibers were found to be composed of oriented amorphous chains and crystal seeds; the partially complete crystallization process tended to be more complete in the case of lower chamber pressures. Annealing markedly promoted the growth of oriented crystallites along the fiber axis. In addition, we were able to determine the relationship between the oriented crystallites and the morphologies of the obtained nanofibers. CLSD is a novel technique for preparing nanofibers and can be used to fabricate nanofibers of various highly chemically resistant thermoplastics such as PPS. PPS is not known to dissolve in any solvent at room temperature and is highly heat resistant as well, having a melting point of 280°C, which is much higher than that of PET (260°C), the material previously drawn using CLSD. CLSD allowed for the preparation of PPS nanofibers using only CO_2 laser irradiation without requiring any other processes or solvents.

ACKNOWLEDGMENTS

The authors are grateful to Dr. A. Kato (Nissan Arc, Ltd.) for stimulating discussions. We are also grateful to Polyplastics Co., Ltd. for providing the PPS samples.

REFERENCES

1. Hill, J. H. W.; Brady, D. G. *Polym. Eng. Sci.* **1976**, *16*, 831.
2. Leonardo, C. L.; Wilkes, G. L. *J. Macromol. Sci., Part C: Polym. Rev.* **1998**, *29*, 83.
3. Yeo, Y. J.; Jeon D. W.; Kim, C. S.; Choi, S. H.; Cho, K.-S.; Lee, Y. K.; Kim, C. K. *J. Mater. Res. Part B: Appl. Biomater.* **2005**, *72*, 86.
4. Meng, J.; Song, L.; Meng, J.; Kong, H; Zhu, G.; Wang, C.; Xu, L.; Xie, S.; Xu, H. *J. Mater. Res. Part B: Appl. Biomater.* **2006**, *79*, 298.
5. Boland, E. D.; Telemeco, T. A.; Simpson, D. G.; Wnek, G. E.; Bowlin, L. *J. Mater. Res. Part B: Appl. Biomater.* **2004**, *71*, 144.
6. Ding, B.; Kimura, E.; Sato, T.; Fujita, S.; Shiratori, S. *Polymer* **2004**, *45*, 1895.
7. Gupta, P.; Wilkes, G. L. *Polymer* **2003**, *44*, 6353.
8. Ayutsede, J.; Ghandi, M.; Sukigara, S.; Micklus, M.; Chen, H. E.; Ko, F. *Polymer* **2005**, *46*, 1625.
9. Fong, H. *Polymer* **2004**, *45*, 2427.
10. Kim, J. S.; Reneker, D. H. *Polym. Eng. Sci.* **1999**, *39*, 849.
11. Deitzel, J. M.; Kleinmeyer, J.; Harris, D.; Tan, B. N. C. *Polymer* **2001**, *42*, 261.
12. Pedicini, A.; Farris, R. *J. Polymer* **2003**, *44*, 857.
13. Varabhas, J. S.; Chase, G. G.; Reneker, D. H. *Polymer* **2008**, *49*, 4226.

14. Zhou, H.; Green, T. B.; Joo, L. Y. *Polymer* **2006**, *47*, 7497.
15. Dalton, P. D.; Grafahrend, D.; Klinkhammer, K.; Klee, D.; Möller, M. *Polymer* **2007**, *23*, 6823.
16. Lyons, J.; Li, C.; Ko, F. *Polymer* **2004**, *45*, 7597.
17. Ellison, C. J.; Phatak, A.; Giles, D. W.; Macosko, C. W.; Bates, F. S. *Polymer* **2007**, *11*, 3306.
18. Raghavendra, R. H.; Gajanan, S. B. *J. Appl. Polym. Sci.* **2009**, *115*, 1062.
19. Raghavendra, R. H.; Gajanan, S. B. *J. Appl. Polym. Sci.* **2010**, *118*, 3144.
20. Boker, S.; Gu, B.; Dirmer, M.; Delicado, R.; Sen, A.; Jackson, B.-R.; Badding, J.-V. *Polymer* **2006**, *47*, 8337.
21. Hong, K. H.; Kang, T. J. *J. Appl. Polym. Sci.* **2006**, *100*, 167.
22. Nakata, K.; Fujii, K.; Ohkoshi, Y.; Gotoh, Y.; Nakamura, M.; Numata, M.; Kamiyama, M. *Macromol. Rapid Commun.* **2007**, *28*, 792.
23. Suzuki, A.; Aoki, K. *Eur. Polym. J.* **2008**, *44*, 2499.
24. Suzuki, A.; Yamada, Y. *J. Appl. Polym. Sci.* **2010**, *116*, 1913.
25. Suzuki, A.; Arino, K. *Eur. Polym. J.* **2012**, *48*, 1169.
26. Maemura, E.; Cakmak, M.; White, L.-J. *Polym. Eng. Sci.* **1989**, *29*, 140.
27. Leonardo, C. L.; Garth, L. W. *J. Polym. Sci. Part C: Polym. Lett.* **1986**, *24*, 573.
28. Suzuki, A.; Tanizawa, K. *Polymer* **2009**, *50*, 913.
29. Suzuki, A.; Khono, T.; Kunugi, T. *J. Polym. Sci. Part B: Polym. Phys.* **1998**, *10*, 1731.
30. Cheng, S. Z. D.; Wu, Z. Q.; Wunderlich, B. *Macromolecule* **1987**, *20*, 2802.
31. Lu, J.; Huang, R.; Oh, I.-K. *Macromol. Chem. Phys.* **2007**, *208*, 4, 405.
32. Tabor, B. J.; Marge, E. P.; Boo, J. *Eur. Polym. J.* **1971**, *7*, 1127.